Electrodynamics of two-dimensional materials

Majérus, Bruno; Dremetsika, Evdokia; Lobet, Michaël; Henrard, Luc; Kockaert, Pascal

Published in:
Physical review. B

DOI:
10.1103/physrevb.98.125419

Publication date:
2018

Document Version
Publisher's PDF, also known as Version of record

Electrodynamics of two-dimensional materials: Role of anisotropy

Bruno Majérus,[1] Evdokia Dremetsika,[2] Michaël Lobet,[1,3] Luc Henrard,[1] and Pascal Kockaert[2,*]

[1]*Department of Physics and Namur Institute of Structured Matters, University of Namur, 61 rue de Bruxelles, B-5000 Namur, Belgium*

[2]*OPERA-photonics, Université libre de Bruxelles, 50 Avenue F. D. Roosevelt, Code Postal 194/5, B-1050 Bruxelles, Belgium*

[3]*John A. Paulson School of Engineering and Applied Sciences, Harvard University, 9 Oxford Street, Cambridge, Massachusetts 02138, USA*

(Received 23 July 2018; published 21 September 2018)

Two-dimensional (2D) materials are intrinsically anisotropic, and an accurate description of their out-of-plane response to an electromagnetic field is more and more important as new materials with diverse properties are proposed. Their electromagnetic properties are often modeled using a single sheet with a surface susceptibility or conductivity or by means of a thin film of finite thickness with an effective bulk permittivity. The discordances between these two approaches lead to two irreconcilable interpretations of the optical characterizations and uncertain predictions of electromagnetic responses. Here, we fully account for the particular anisotropy of 2D materials and reconcile both approaches. We propose a unified description for the electromagnetic properties that applies to 2D heterostructures for all polarizations and at all angles of incidence. In particular, we determine the class of materials for which both models can be used indifferently and when particular care should be taken to select the thickness and the tensorial response of the effective thin film. We illustrate our conclusions on extensively studied experimental quantities such as transmittance and ellipsometric data of graphene and metal dichalcogenides. We discuss similarities and discrepancies reported in the literature when single-sheet or thin-film models are used.

DOI: 10.1103/PhysRevB.98.125419

I. INTRODUCTION

The electromagnetic (EM) properties of two-dimensional (2D) materials are at the forefront of current research activities. Further developments for applications as diverse as optical modulators, transparent conductive films, photovoltaic systems, superabsorbers, and sensors require an accurate description of their electromagnetic response [1–4]. For example, optical contrast and transmission are among the commonly used quantities to characterize 2D systems, in particular, to determine their thickness or their number of layers [5–9]. Furthermore, electromagnetic properties are the macroscopic fingerprints of elementary excitations such as the interband transition, excitons, and plasmons. Their correct analysis is therefore crucial for the understanding of the underlying physics of 2D materials.

Several models are commonly used for the EM response of 2D materials. First, a purely 2D system with the definition of a single-sheet (surface) conductivity σ^s or susceptibility χ^s [10,11] has been proposed. In particular, for graphene, an analytical expression for σ^s based on the tight-binding approximation and Kubo formula has become popular [12]. It provides a clear distinction between interband and intraband electronic transitions. The surface conductivity can be determined experimentally, e.g., via Brewster angle measurements [13].

Using another approach, 2D materials have been considered as isotropic materials with a small but finite thickness [7–9,14,15]. This approach notably allows using the well-developed transfer matrix technique to predict and interpret optical data (including ellipsometry) with widely available methodology and numerical codes. The thickness is often arbitrarily taken to be the interlayer distance of the three-dimensional (3D) counterpart of the 2D material [11,16], considered as a fitting parameter [7] or evaluated based on the variation of the electronic density in the transverse direction [17].

These two approaches (a purely 2D surface conductivity and a 3D isotropic thin film) do not always match, as demonstrated analytically and numerically [18,19], and a model-dependent interpretation of ellipsometric data has been reported [20]. This is particularly true for oblique incidence and TM (p-polarized) EM radiation [21]. Indeed, considering only a purely in plane 2D conductivity means that the out-of-plane response of the layer is neglected, while for an isotropic thin film, both the in-plane and out-of-plane responses are linked. Very recently, a criterion has been proposed to determine in which conditions the two models give similar results at normal incidence [22].

Anisotropic thin films have also been studied. The out-of-plane component has been taken to be a free parameter [20,23,24] or deduced from first-principles-approach calculations performed with periodic boundary conditions [19,25]. The out-of-plane susceptibility in a single-sheet model was recently considered by two of us to analyze the nonlinear optical response of graphene [26]. Such an adequate description of the out-of-plane component is of prime necessity since very diverse 2D materials with potentially large out-of-plane polarizabilities are synthesized [27] and predicted [28].

*pascal.kockaert@ulb.ac.be

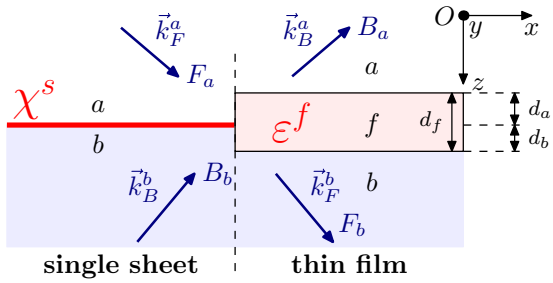

FIG. 1. Schematic representation of the two configurations. Left: current sheet model. Right: thin film with an effective material f extending over a distance d_a (d_b) on the a (b) side. The wave vectors of the forward F and backward B fields in media a and b are denoted by $\vec{k}^{a,b}_{F,B}$. The reference frame is $Oxyz$.

In this work, we study analytically and numerically the conditions of the EM response function (surface susceptibility, dielectric tensor) and of the thickness of the effective thin film for a correct description of the response of 2D materials. In particular, we analytically link the surface susceptibility of the single sheet to the ordinary and extraordinary optical constants of the equivalent thin film. We then focus our attention on the determination of the surface conductivity of the 2D materials based on the interpretation of optical transmission, ellipsometry, and optical contrast measurements.

II. MODELIZATION OF 2D MATERIALS

In this section, we perform a comparison between the single-sheet and thin-film approaches within the framework of transfer matrix formalism for stratified media [29]. As a first step, we build the transfer matrix of a single sheet at the interface of two surrounding media (a and b), as depicted in Fig. 1 (left). In a second step, we calculate the transfer matrix of a thin film with finite thickness d_f (Fig. 1, right). We then analytically compare the two approaches and highlight the consequences for quantities that can be easily determined experimentally (transmittance, ellipsometric data, optical contrast). Importantly, we insist here on the consequences of the intrinsic anisotropy of 2D materials.

The single sheet is described by a surface susceptibility tensor $\overline{\chi}^s$ that is diagonal in our reference frame (Fig. 1). The in-plane components of $\overline{\chi}^s$ are directly related to its surface conductivity by

$$\sigma^s_\alpha = -i\varepsilon_0\omega\chi^s_\alpha, \tag{1}$$

where $\alpha = x, y$. The out-of-plane component χ^s_z is also considered here, but an out-of-plane conductivity has no physical meaning for a single sheet.

The thin-film material is described by a dielectric tensor $\overline{\varepsilon}^f$ related to the bulk conductivity components by

$$\varepsilon^f_{\alpha\beta} = \left(\varepsilon_0 + \frac{i\sigma_\alpha}{\omega}\right)\delta_{\alpha\beta}. \tag{2}$$

The in-plane and bulk conductivities are related by $\sigma^s_\alpha = d_f\,\sigma_\alpha$ [19]. The incident and substrate materials (a and b) can be anisotropic but with their optical axes aligned with those of the 2D material, i.e., $\varepsilon^{a,b}_{\alpha\beta} = \varepsilon_0\varepsilon^{a,b}_\alpha\delta_{\alpha\beta}$, which is the case in most (if not all) of the systems studied experimentally so far. This hypothesis avoids the coupling between transverse-electric (TE) and transverse-magnetic (TM) modes. We allow those surrounding materials to have a complex permittivity and express the dependence on the angle of incidence via the wave vector $\vec{k} = (k_x, k_y, k_z)$. If the incident medium is a perfect dielectric characterized by the real isotropic permittivity $\varepsilon_0\varepsilon_a = \varepsilon_0 n_a^2$ and $k_y = 0$, we have $k_x = k_0\, n_a \sin\alpha_i$, with k_0 being the wave number of the light in vacuum, n_a being the refractive index of medium a, and α_i being the angle of incidence.

TABLE I. Definition of the coefficients in TE and TM configurations to first order in $\varphi_x, \varphi_y, \varphi_z$. In these expressions, m and n will be replaced by a, b, and f to denote, respectively, the incidence medium, the substrate, and the thin film. The forward (backward) component F_m (B_m) is defined in each medium m with respect to the forward (backward) component of the electric field parallel to the interface $[E^m_{x,y}]_F$ ($[E^m_{x,y}]_B$), with y for TE and x for TM.

	TE (s polarization)	TM (p polarization)
k_0	ω/c	
k_x	in-plane component of input $\vec{k}$	
k^m_z	$\sqrt{\varepsilon^m_y k_0^2 - k_x^2}$	$\sqrt{\varepsilon^m_x(k_0^2 - k_x^2/\varepsilon^m_z)}$
F_m	$[E^m_y]_F$	$\varepsilon^m_x/k^m_z[E^m_x]_F$
B_m	$[E^m_y]_B$	$-\varepsilon^m_x/k^m_z[E^m_x]_B$
t	F_b/F_a	
r	B_a/F_a	
α_{mn}	k^n_z/k^m_z	$(\varepsilon^m_x k^n_z)/(\varepsilon^n_x k^m_z)$
t_{mn}	$2/(1+\alpha_{mn})$	
r_{mn}	$t_{mn} - 1$	
φ_x	0	$\frac{k^a_z k^b_z}{\varepsilon^b_x k^a_z + \varepsilon^a_x k^b_z}\chi^s_x$
φ_y	$\frac{k_0^2}{k^a_z + k^b_z}\chi^s_y$	0
φ_z	0	$\frac{k_x^2}{\varepsilon^b_x k^a_z + \varepsilon^a_x k^b_z}\frac{\varepsilon^a_x \varepsilon^b_x}{\epsilon_{ab}}\chi^s_z$
ϵ_{ab}	$\frac{2}{(1/\varepsilon^a_z + 1/\varepsilon^b_z)}$	
$\varphi_\pm$	$\varphi_x \pm (\varphi_y + \varphi_z)$	
χ^s_{jj}	$i\sigma^s_{jj}/(\varepsilon_0\omega)$	

A. Two-dimensional material as a single sheet

In order to describe the out-of-plane component in the single-sheet model, we use the approach described in Ref. [26] based on Refs. [30,31]. In particular, the transmission coefficient t and the reflection coefficient r of the electric field in TE and TM configurations can be written as (see the Supplemental Material [32])

$$t = t_{ab}[1 + i(\varphi_x + \varphi_y + \varphi_z)], \tag{3}$$

$$r = t - 1 - 2i\varphi_x, \tag{4}$$

with the parameters defined in Table I. We note that t_{ab}, which is the transmission coefficient in the absence of a 2D material, depends on the propagation direction and is therefore

not symmetrical, i.e., $t_{ba} = 2 - t_{ab}$, while $\varphi_x, \varphi_y, \varphi_z$ do not depend on the propagation direction.

In these notations the transfer matrix between the incident medium a and the outgoing medium (substrate) b can be written as (see the Supplemental Material [32])

$$\mathcal{S}_{ab} = \frac{1}{t_{ab}}\begin{pmatrix} 1 - i\varphi_+ & r_{ab} + i\varphi_- \\ r_{ab} - i\varphi_- & 1 + i\varphi_+ \end{pmatrix}, \tag{5}$$

so that the forward (F) and backward (B) field components in media a and b at the single-sheet interface are linked by

$$\begin{pmatrix} F_a \\ B_a \end{pmatrix} = \mathcal{S}_{ab}\begin{pmatrix} F_b \\ B_b \end{pmatrix}. \tag{6}$$

The expressions for TE and TM modes have a similar form if the forward and backward components are defined as in Table I. The matrix $\mathcal{S}_{ab}$ includes the out-of-plane response of the current sheet χ_z^s through φ_z and can therefore be compared to the thin-film model.

B. Two-dimensional material as a thin film

The transfer matrix $\mathcal{T}_{ab}$ that describes the propagation of EM waves in the effective thin-film system of thickness d_f with the diagonal permittivity tensor $\overline{\varepsilon}^f$ of components $\varepsilon_x^f, \varepsilon_y^f$, and ε_z^f involves the transfer matrix at the two interfaces ($\mathcal{I}_{af}$ and $\mathcal{I}_{fb}$) and the propagation matrix $\mathcal{P}_f$ in the homogeneous film f over a distance d_f. Then

$$\mathcal{T}_{ab} = \mathcal{I}_{af}\mathcal{P}_f\mathcal{I}_{fb}, \tag{7}$$

with

$$\mathcal{P}_m = \begin{pmatrix} \mathrm{e}^{-\mathrm{i}\Phi_m} & 0 \\ 0 & \mathrm{e}^{\mathrm{i}\Phi_m} \end{pmatrix}, \tag{8}$$

$$\mathcal{I}_{mn} = \frac{1}{t_{mn}}\begin{pmatrix} 1 & r_{mn} \\ r_{mn} & 1 \end{pmatrix}, \tag{9}$$

where $\Phi_m = k_z^m d_m$, d_m is the thickness of layer m, and k_z^m, r_{mn}, and t_{mn} are defined in Table I. The anisotropy of the media is accounted for through the diagonal components of the dielectric tensors.

C. Analytical comparison

The two models are considered equivalent if their transfer matrices are identical. However, we cannot directly compare $\mathcal{S}_{ab}$ and $\mathcal{T}_{ab}$ since the propagation in the slab of thickness $d_f = d_a + d_b$ is not considered in $\mathcal{S}_{ab}$. The correct equality is then

$$\mathcal{T}_{ab} = \mathcal{P}_a\mathcal{S}_{ab}\mathcal{P}_b. \tag{10}$$

In the limit of small phase shift, we can develop (10) to first order in $k_0 d_f$ for the bulk parameters ($\Phi_a, \Phi_b, \Phi_f \ll 1$) and to first order in $k_0\chi^s$ for the single-sheet parameters ($\varphi_x, \varphi_y, \varphi_z \ll 1$). A lengthy but straightforward calculation provides the effective dielectric function of the thin film as

$$\varepsilon_x^f = \chi_x^s/d_f + \eta_a\varepsilon_x^a + \eta_b\varepsilon_x^b, \tag{11}$$

$$\varepsilon_y^f = \chi_y^s/d_f + \eta_a\varepsilon_y^a + \eta_b\varepsilon_y^b, \tag{12}$$

$$\frac{1}{\varepsilon_z^f} = \frac{\eta_a}{\varepsilon_z^a} + \frac{\eta_b}{\varepsilon_z^b} - \frac{\chi_z^s}{\epsilon_{ab}\, d_f}, \tag{13}$$

where $\eta_a = d_a/d_f$ and $\eta_b = d_b/d_f$ and then $\eta_a + \eta_b = 1$ (Fig. 1). As expected, the effective dielectric tensor components do not depend on the angle of incidence. Nevertheless, those quantities depend on the 2D material through χ^s and on the geometry of the thin film defined by d_a and d_b. More surprisingly, the components of the dielectric tensor of the surrounding materials $\overline{\varepsilon}^a$ and $\overline{\varepsilon}^b$ also appear in (11)–(13). In the frequent case where the incident medium is air and a thin film of thickness d_f is lying on top of the substrate b, we have $d_a = d_f$, $d_b = 0$, and $\varepsilon_i^a = 1$, so that

$$\varepsilon_x^f = \chi_x^s/d_f + 1, \tag{14}$$

$$\varepsilon_y^f = \chi_y^s/d_f + 1, \tag{15}$$

$$\frac{1}{\varepsilon_z^f} = 1 - \frac{1 + \varepsilon_z^b}{2\varepsilon_z^b d_f}\chi_z^s. \tag{16}$$

Equations (14) and (15) are commonly used for 2D materials and are perfectly valid under the assumptions reported above. The relation (16) for the out-of-plane components still includes ε_z^b and is far from being intuitive but is important to understand the link between the isotropic thin film and the anisotropic single-sheet models. Indeed, it explains some discrepancies between the two approaches reported in the literature, as we will discuss later. In the absence of out-of-plane susceptibility ($\chi_z^s = 0$), (16) gives $\varepsilon_z^f = 1$, and the effective thin film is anisotropic.

III. DISCUSSION

In this section we compare the results of the two approaches for quantities that are easily obtained experimentally: transmittance, ellipsometry, and optical contrast. A perfect planar interface between the different media is considered. In cases where the surface roughness of the substrate is important, it can be taken into account in the transfer matrix calculation, i.e., by considering an intermediate thin layer with an effective dielectric response [33].

A. Transmittance

We consider a sample with the geometry depicted in Fig. 1. In the TM configuration, from (3) and Table I, the change in transmittance induced by the 2D material in the small-phase-shift hypothesis (first order in $k_0 d_f \sim k_0\chi^s$) and for real $\overline{\varepsilon}_a$ and $\overline{\varepsilon}_b$ is

$$\left|\frac{t}{t_{ab}}\right|^2 - 1 = -t_{ab}\frac{k_z^b}{\varepsilon_x^b}\mathrm{Im}\chi_x^s\left[1 + \frac{k_x^2}{k_z^a k_z^b}\frac{\varepsilon_x^a\varepsilon_x^b}{\epsilon_{ab}}\left(\frac{\mathrm{Im}\chi_z^s}{\mathrm{Im}\chi_x^s}\right)\right] \tag{17}$$

$$= -t_{ab}\frac{k_z^b}{\varepsilon_x^b}\mathrm{Im}\varepsilon_x^f d_f\left[1 + \frac{k_x^2}{k_z^a k_z^b}\frac{\varepsilon_x^a\varepsilon_x^b}{|\varepsilon_z^f|^2}\left(\frac{\mathrm{Im}\varepsilon_z^f}{\mathrm{Im}\varepsilon_x^f}\right)\right]. \tag{18}$$

The change in transmittance (17) is then related only to Im χ^s and, via (1), to Re σ^s. Simple transmittance measurements can therefore not provide information on Re χ^s or Im σ^s. In contrast, both the real and imaginary parts of ε_z^f are present in (18) through $|\varepsilon_z^f|^2$. Similar conclusions are drawn for the reflectance (see Appendix A 2).

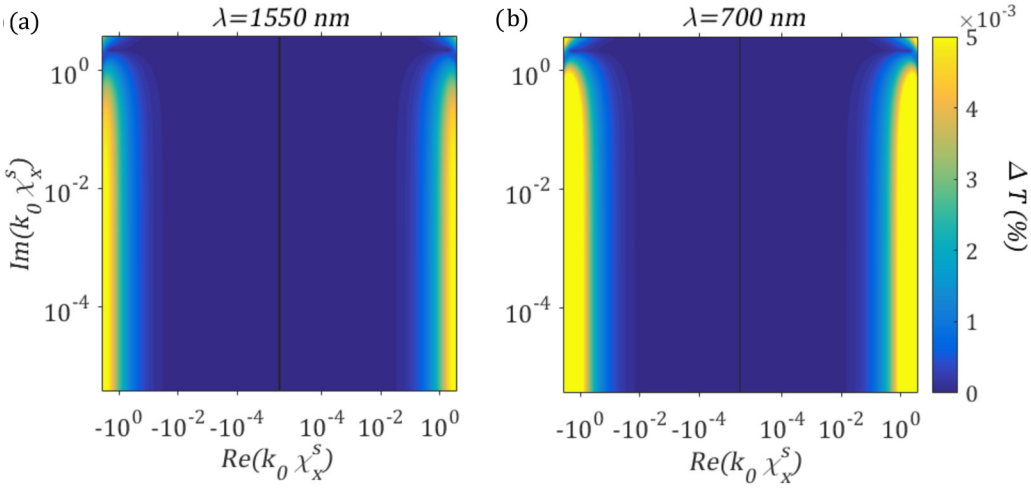

FIG. 2. Relative difference ΔT between the transmittance computed in the single sheet and in the anisotropic thin-film models, with respect to the real and imaginary parts of the single-sheet susceptibility, related to the conductivity by $k_0\chi_x^s = i\sigma_x^s/(\varepsilon_0 c)$. The system considered is air/2D material/glass. The refractive index of glass is taken to be 1.5. (a) Infrared EM radiation ($\lambda = 1550$ nm). (b) Visible light ($\lambda = 700$ nm).

To understand the impact of using the thin-film model instead of the single-sheet approach and to test the validity range of (11)–(13) with respect to $k_0\chi^s$, we have performed extensive numerical simulations. All the numerical results presented here are for a TM wave incident on an air/2D material/glass ($n_b = 1.5$) system with an angle $\theta = 75^\circ$ and a thickness $d_f = 0.34$ nm, unless otherwise specified.

Figure 2 displays the relative difference of transmittance defined as

$$\Delta T = \frac{T_{\rm sh} - T_{\rm tf}}{T_{\rm sh}} \times 100, \tag{19}$$

where the thin-film transmittance $T_{\rm tf}$ is computed from (7) without performing the small-phase-shift approximation and the single-sheet transmittance $T_{\rm sh}$ is calculated using (17). We compare results for two incident wavelengths (in the IR, $\lambda = 1550$ nm, and in the visible, $\lambda = 700$ nm) obtained with the single-sheet model with no out-of-plane susceptibility ($\chi_z^s = 0$) and with the anisotropic thin film with $\overline{\overline{\varepsilon}}^f$ from (11)–(13). The transmittances computed in the *anisotropic* thin-film model and in the single-sheet model are obviously in very good agreement. Therefore, in the following, we will consider that the single-sheet model and the anisotropic thin-film model give equivalent results. This rationalizes also the fact that the small-phase-shift condition is satisfied for a large range of 2D susceptibilities.

When the small-phase-shift condition is relaxed ($|\mathrm{Re}[k_0\chi^s]| \gtrapprox 1$), larger ΔT is obtained, corresponding to the yellow bands on the left and right sides of Figs. 2(a) and 2(b). The difference is larger at smaller wavelengths.

For an isotropic thin-film model more important discrepancies are observed, as illustrated in Fig. 3. Note that the scale of ΔT is different in Figs. 2 and 3. For Fig. 3, ε_x and ε_y are equal

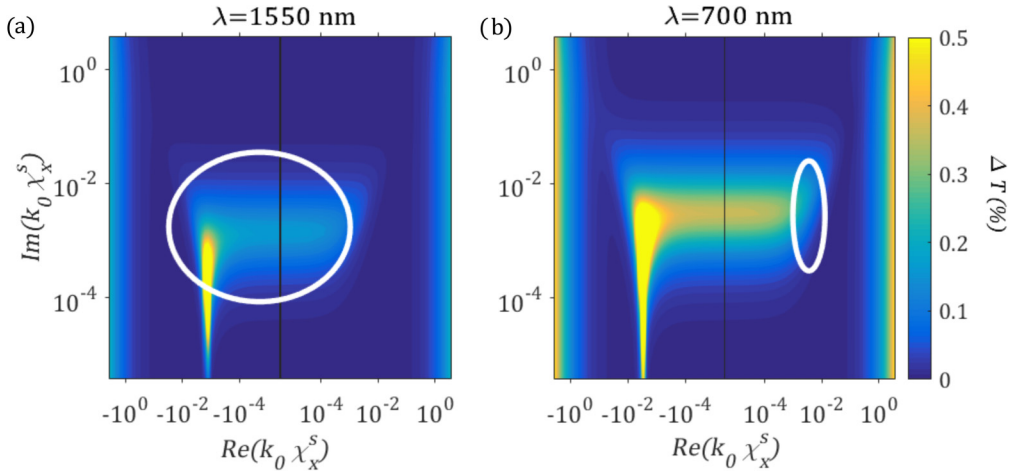

FIG. 3. Same as Fig. 2, but for the isotropic thin-film model. The circled areas indicate graphene's adimensional parameter $k_0\chi^s$. To determine it we use the Kubo formula at a fixed wavelength of (a) 700 nm or (b) 1550 nm over a range of Fermi levels from 0.05 to 1 eV and a range of relaxation times from 10 to 200 fs. Within this range of parameters, an artificial plasmonic resonance appears in the left panel.

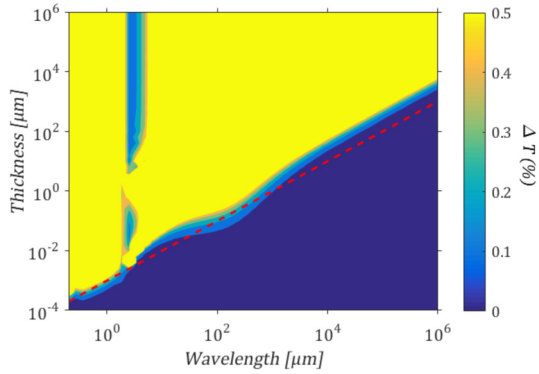

FIG. 4. Difference of transmittance ΔT between the isotropic and anisotropic thin films of graphene for a system of air/graphene/glass. The refractive index of glass is taken to be 1.5. Graphene is modeled using the Kubo formula with $E_F = 0.4\,\text{eV}$, $\tau = 100\,\text{fs}$. The red dashed line represents a thickness equal to 1/1000 of the wavelength.

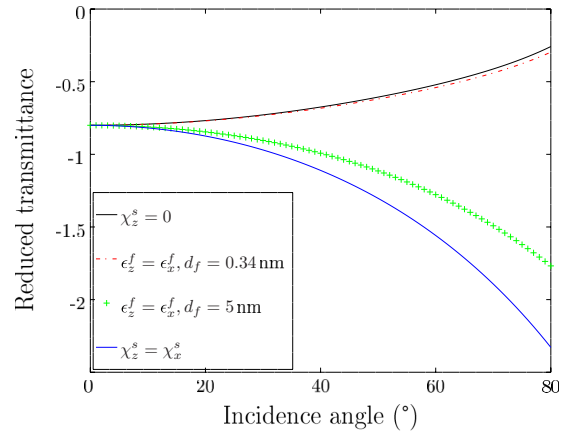

FIG. 5. Reduced transmittance [brackets in (17) and (18)] for an air/graphene/glass structure: $n_a = 1$, $n_b = 1.5$, $\chi_x^s = (1.50 + 2.29i)\,\text{nm}$ at a wavelength of 634 nm [15]. Curves are for the anisotropic single sheet with no out-of-plane response ($\chi_z^s = 0$), the isotropic thin-film model ($\varepsilon_z^f = \varepsilon_x^f$) with $d_f = 0.34\,\text{nm}$ and $d_f = 5\,\text{nm}$, and isotropic current sheet model ($\chi_z^s = \chi_x^s$).

and obtained from (11) and (12), and $\varepsilon_x = \varepsilon_y = \varepsilon_z$. For a better interpretation of the data, we identify in Fig. 3 the range of values for the susceptibility of graphene at each wavelength based on the Kubo formula [12] for a range of Fermi levels from 0.05 to 1 eV and a range of relaxation times from 10 to 200 fs. Note that for the anisotropic case, we observe a particularly small ΔT with a maximum of $2 \times 10^{-3}\%$ in this range.

Notably, a high value of ΔT is observed in a vertical line corresponding to $\text{Re}[\chi^s] = -d_f$, for which the real part of the permittivity $\varepsilon = 1 + \chi^s/d_f$ vanishes. This shows, similar to what was reported in Ref. [21], that an artificial plasmonic resonance is predicted by an *isotropic* thin-film model due to the artificial metallic nature of the out-of-plane component of the permittivity tensor. This unphysical resonance could have dramatic effects on the prediction of the optical properties.

To investigate further the influence of the anisotropy, we present in Fig. 4 the difference between the transmittance obtained with the isotropic and anisotropic thin-film models in the TM configuration for graphene as a function of the incident wavelength and of the thin-film thickness. The two models give very similar results for the ratio $\lambda/d_f > 1000$, i.e., for very small $k_0 d_f$ (under the dashed line). This validates the fact that the anisotropy of graphene has often been disregarded without consequences for the validity of the conclusions if the chosen thickness of the thin film is at least three orders of magnitude lower than the wavelength.

This surprisingly good prediction within the isotropic thin-film model for intrinsically anisotropic 2D material is explained as follows. The isotropic thin-film model does not correspond to the assumption $\chi_z^s = \chi_x^s$ but to $\varepsilon_z^f = \varepsilon_x^f$. By means of (13), this is equivalent to setting

$$\text{Im}\chi^s z = \frac{\epsilon_{ab}}{\left|\varepsilon_z^f\right|^2} d_f \,\text{Im}\varepsilon_z^f = \frac{\epsilon_{ab}}{\left|1 + \chi_x^s/d_f\right|^2} \text{Im}\chi_x^s, \qquad (20)$$

which shows that the isotropic thin-film model tends to the *anisotropic* single-sheet one with $\chi_z^s = 0$ when $|\chi_x^s|^2 \gg d_f^2$, as in this case (20) provides $\chi_z^s \approx 0$.

This explains that the isotropic thin-film model can be used with good results to model graphene with $\text{Im}[\chi_z^s] = 0$ and $d_f = 0.34\,\text{nm}$. In particular, it confirms that in the limit $d_f = 0$, both models agree, as reported in Ref. [34]. More importantly, this also resolves the apparent contradiction between the conclusions of Ref. [34] and those of Refs. [18,19,21] on the equivalence (or not) of both models for $d_f \to 0$. Indeed, (20) shows that, if we model graphene by means of a thicker layer so that $\chi_x^s \ll d_f \ll 1/k_0$, the isotropic thin-film model corresponds to the *isotropic* single-sheet one ($\chi_x^s = \chi_z^s$ in the particular case where $n_a = n_b = 1$) and not to the *anisotropic* single sheet with $\chi_z^s = 0$. We illustrate this analytical observation in Fig. 5, where we plot the terms in brackets in (17) and (18) for an air/graphene/glass system at 634 nm as a function of the angle of incidence for different approaches: the single sheet for $\chi_z^s = 0$ (solid black line) and with $\chi_x^s = \chi_z^s$ (dashed blue line) and the isotropic thin film for $d_f = 0.34\,\text{nm}$ (dot-dashed red line) and $d_f = 5\,\text{nm}$ (green crosses). The results for the anisotropic thin film cannot be distinguished from those of the anisotropic single sheet and are therefore not plotted. The thickness $d_f = 5\,\text{nm}$ is commonly used in discrete numerical simulations to avoid prohibitive numerical cost [21]. As expected, at normal incidence, all curves are superimposed, and the anisotropy does not play a role. As the angle of incidence increases, the z component of the response functions becomes more important, and the exact value of the thickness of the thin film influences the computed optical properties. Surprisingly, isotropic thin-film calculations correspond to either an isotropic or anisotropic single-sheet model depending on the considered effective thickness.

To conclude on the physical quantities that can be deduced from transmittance measurements, we note that, although transmittance measurements at different angles allow us, in principle, to separate the in-plane and out-of-plane responses

of the imaginary part of the susceptibility (the real part of the conductivity), these measurements are usually performed at normal incidence, for which the TE and TM cases coincide.

B. Ellipsometry

Ellipsometry records the ratio of the reflection or transmission of a sample in TM and TE configurations at different angles. Considering again a sample with the geometry depicted in Fig. 1, from Eqs. (3) and (4), still in the small-phase approximation (i.e., to first order in $k_0\chi^s$), we get

$$\frac{\rho^t}{\rho_0^t} = \frac{t^{\mathrm{TM}}}{t_{ab}^{\mathrm{TM}}}\frac{t_{ab}^{\mathrm{TE}}}{t^{\mathrm{TE}}} = \left[1 + i\left(\varphi_x^{\mathrm{TM}} - \varphi_y^{\mathrm{TE}} + \varphi_z^{\mathrm{TM}}\right)\right], \tag{21}$$

with ρ^t being the ellipsometric ratio with the 2D material and ρ_0^t being the same ratio for the interface without the 2D material. Under the assumption that $\chi_x^s = \chi_y^s$, using Table I, we can write

$$\frac{\rho^t}{\rho_0^t} - 1 = -\frac{ik_x^2}{\varepsilon_x^a k_z^b + \varepsilon_x^b k_z^a}\left(\chi_x^s - \frac{\varepsilon_x^a \varepsilon_x^b}{\epsilon_{ab}}\chi_z^s\right). \tag{22}$$

The in-plane χ_x^s and out-of-plane χ_z^s susceptibilities then cannot be separated by means of standard transmission ellipsometry as the coefficient $(\varepsilon_x^a\varepsilon_x^b/\epsilon_{ab})$ in front of χ_z^s is independent of k_x and k_z and therefore the angle of incidence.

In order to analyze these results further, it is convenient to define the term in parentheses in (22) as

$$\chi^{\mathrm{ell}} = \chi_x^s - \frac{\varepsilon_x^a \varepsilon_x^b}{\epsilon_{ab}}\chi_z^s, \tag{23}$$

which contains all the dependence on the susceptibility. We note that the same dependence is found for reflection ellipsometry (see Appendix A 3).

We can here provide a simple explanation for the difference reported in Ref. [20] between the susceptibilities extracted from ellipsometric data using different models for MoS_2 on a glass substrate. We denote $[\chi_x^s]_i$ as the in-plane susceptibility deduced from the isotropic thin-film model with $d_f = 0.615$ nm (Fig. 6, blue curve with crosses) and $[\chi_x^s]_a$ as the one found with the anisotropic single-sheet model [Fig. 6 ($\chi_z^s = 0$), red curve with squares].

For the isotropic thin film, using (16),

$$\chi^{\mathrm{ell}} = \left[\chi_x^s\right]_i\left(1 - \frac{\varepsilon_x^b}{1 + \left[\chi_x^s\right]_i/d_f}\right), \tag{24}$$

while for the anisotropic sheet, we simply get

$$\chi^{\mathrm{ell}} = \left[\chi_x^s\right]_a. \tag{25}$$

Comparing the last two equations, we obtain

$$\left[\chi_x^s\right]_a = \left[\chi_x^s\right]_i - \varepsilon_x^b d_f + \frac{\varepsilon_x^b d_f}{1 + \left[\chi_x^s\right]_i/d_f}. \tag{26}$$

The inset of Fig. 6 displays the difference between $[\chi_x^s]_i$ and $[\chi_x^s]_a$ and compares it with $-\varepsilon_x^b d_f$. The small discrepancy between the two curves shows that the last term in (26) is very small, as the main difference between $[\chi_x^s]_a$ and $[\chi_x^s]_i$ comes from the real quantity $-\varepsilon_x^b d_f$. This occurs because $d_f \ll |\chi_x^s|$ over the whole spectral range. As a result, (26) predicts that, for MoS_2, the imaginary part of χ_x^s does not depend significantly on the anisotropy of the model. This is in agreement with what was reported in Ref. [20], where the curves for the conductivity (imaginary part of the complex susceptibility) are very similar in the two approaches. This good agreement between experimental data and the analytical predictions again confirms the validity of the small-phase-shift approximation ($k_0\chi^s \ll 1$).

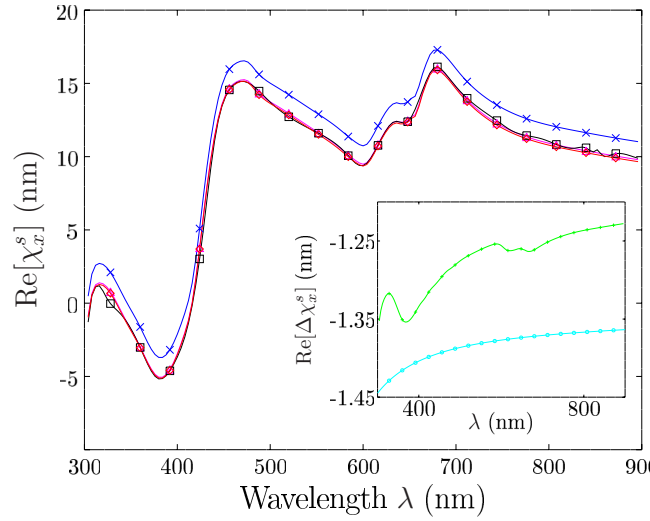

FIG. 6. Values of $\mathrm{Re}[\chi_x^s]$ for a MoS_2 single layer retrieved with the isotropic thin-film model ($[\chi_x^s]_i$, blue curve and crosses) and the anisotropic current sheet model ($[\chi_x^s]_a$, black curve and squares). Data are from Ref. [20]. The red curve (diamonds) is calculated from $[\chi_x^s]_i$ shifted by $-\varepsilon_x^b d_f$ and is almost superimposed on the black curve. The inset displays the difference $[\chi_x^s]_i - [\chi_x^s]_a$ (green curve with pluses) and $-\varepsilon_x^b d_f$ (cyan curve with circles). The dielectric function of N-BK7 glass (substrate used in Ref. [20]) is taken from Sellmeier's equation provided by Schott [35].

We conclude that standard ellipsometry provides no information on the x-z anisotropy of the 2D sample. It is, however, important to note that the single-sheet approach imposes implicitly $\chi_z^s = 0$, while the isotropic thin-film approach assumes $\chi_z^s = \epsilon_{ab}\chi_x^s/\varepsilon_x^f$, which explains the differences reported in the literature for the retrieval of χ_x^s from ellipsometric data. Equation (23) allows us to introduce in the fitting procedure a value for χ_z^s based on theoretical assumptions or obtained experimentally, for example, by means of contrast ratio measurements.

C. Optical contrast

The optical contrast of 2D materials on a thick substrate is often very small and hardly measurable. However, reflection microscopy and optical contrast are commonly used to determine the presence of 2D materials (or the number of layers) if a thin dielectric film is lying on top of the substrate, most often SiO_2 on Si [5,6,36]. This additional layer creates interferences that depend on the 2D susceptibility and allow us to tune the total reflectance of the system. Measurements are usually performed at normal incidence, so that only the in-plane susceptibility is probed. To take into account the additional layer, we should simply multiply $\mathcal{T}_{ab}$ in (10) by

a propagation matrix accounting for the propagation in the additional layer and an interface matrix between this layer and the substrate. As the matrix $\mathcal{T}_{ab}$ is the same in the current sheet and thin-film approaches, the final result does not depend on the chosen model, especially at normal incidence for which the isotropic and anisotropic thin-film models are equivalent.

The optical contrast then depends on the real and imaginary parts of the in-plane susceptibility of the 2D material. However, this measurement is strongly dependent on the parameters of the top layer, including their thickness and permittivity. This probably explains the differences in fitting experimental data that were reported in Ref. [18].

IV. CONCLUSIONS

We have explored analytically and numerically the link between the description of a 2D material with a current sheet and a thin-film model. We have focused our analysis on the description of the intrinsic anisotropy of the layers, i.e., the effect of the out-of-plane component of the single-sheet susceptibility or the out-of-plane component of the dielectric tensor of the thin film. The analytical equivalence in the small-phase-shift condition shows that most discrepancies between these two approaches do not come from the finite thickness of the thin film, but from an incorrect description of the anisotropy, mainly for TM polarization and oblique incidence. In particular, we have shown that considering an isotropic dielectric function of a thin film is not equivalent to assuming an isotropic single-sheet susceptibility. We have also commented on the fact that a single sheet with a vanishing out-of-plane response (as graphene) corresponds to an isotropic or anisotropic effective thin film depending on the effective thickness of the film.

The application of the transfer matrix approach to classical measurement schemes provides evidence that a combination of different techniques is needed to fully characterize a 2D material on a substrate, as depicted on Fig. 1: (1) transmittance measurements on a dielectric substrate provide $\mathrm{Im}[\chi_x^s]$ at normal incidence and could provide $\mathrm{Im}[\chi_z^s]$ at other incidences, and (2) standard ellipsometry, in transmission or reflection, cannot separate the in-plane and out-of-plane contributions. However, combined with transmittance changes, it could provide $\mathrm{Im}[\chi_z^s]$. Another way to retrieve χ_x^s and χ_z^s separately would be to perform ellipsometry experiments on different substrates. Optical contrast on a multilayer substrate combined with the previous methods can also provide information about $\mathrm{Re}[\chi_x^s]$ or even $\mathrm{Re}[\chi_z^s]$ at oblique incidence. We hope that the present single-sheet transfer matrix approach and the analytical connection with the thin-film model will help us to efficiently perform the analysis of stratified media involving 2D materials either for the characterization of 2D materials or for their use in various applications.

ACKNOWLEDGMENTS

Part of this research was performed while E.D. was funded by the Fund for Research Training in Industry and Agriculture (FRIA, Belgium) and the Fonds Van Buuren/Jaumotte-Demoulin and M.L. was a recipient of a fellowship of the Belgian American Educational Foundation. This research used resources of the Plateforme Technologique de Calcul Intensif (PTCI) located at the University of Namur, Belgium, which is supported by the F.R.S.-FNRS under Convention No. 2.4520.11. The PTCI is a member of the Consortium des Équipements de Calcul Intensif (CÉCI).

APPENDIX: DETAILED EXPRESSIONS FOR FITTING EXPERIMENTAL PARAMETERS

In this appendix, we collect the detailed expressions of the reflectance, transmittance, and ellipsometric ratios that can be used for fitting experimental data and separate the different components of the susceptibility tensor. Surrounding media are assumed to be perfect isotropic dielectrics with real susceptibilities.

1. Transmittance

In the TM configuration, the ratio of the transmittance of the substrate with the 2D material T to the transmittance of the bare substrate T_0 is given by

$$\left[\frac{T}{T_0}\right]_{\mathrm{TM}} = 1 - \frac{2\,\mathrm{Im}[\chi_x]}{\varepsilon_x^a/k_z^a + \varepsilon_x^b/k_z^b} - \frac{k_x^2}{\epsilon_{ab}}\frac{2\,\mathrm{Im}[\chi_z]}{k_z^a/\varepsilon_x^a + k_z^b/\varepsilon_x^b}, \tag{A1}$$

In TE configuration, we find

$$\left[\frac{T}{T_0}\right]_{\mathrm{TE}} = 1 - 2k_0^2\frac{\mathrm{Im}[\chi_y]}{k_z^a + k_z^b}. \tag{A2}$$

2. Reflectance

Similarly, for the reflectance ratio, we find

$$\left[\frac{R}{R_0}\right]_{\mathrm{TM}} = 1 - 4\frac{k_z^a\varepsilon_x^a}{\left(\varepsilon_x^a k_z^b\right)^2 - \left(\varepsilon_x^b k_z^a\right)^2} \times \left[\left(k_z^b\right)^2\mathrm{Im}[\chi_x] - \frac{k_x^2}{\epsilon_{ab}}\left(\varepsilon_x^b\right)^2\mathrm{Im}[\chi_z]\right], \tag{A3}$$

$$\left[\frac{R}{R_0}\right]_{\mathrm{TE}} = 1 - 4k_z^a k_0^2\frac{\mathrm{Im}[\chi_y]}{\left(k_z^a\right)^2 - \left(k_z^b\right)^2}. \tag{A4}$$

3. Ellipsometric ratios

Here, we provide the quotient of the ellipsometric ratios ρ and ρ_0 obtained, respectively, on a substrate with and without a 2D material. This is a complex quantity. In the transmission configuration, we get (22), reproduced here for completeness,

$$\frac{\rho^t}{\rho_0^t} = 1 - \frac{ik_x^2}{\varepsilon_x^a k_z^b + \varepsilon_x^b k_z^a}\left(\chi_x^s - \frac{\varepsilon_x^a\varepsilon_x^b}{\epsilon_{ab}}\chi_z^s\right), \tag{A5}$$

while the reflection configuration provides

$$\frac{\rho^r}{\rho_0^r} = 1 + 2i\frac{\varepsilon_x^b k_z^a k_x^2}{\left(\varepsilon_x^a k_z^b\right)^2 - \left(\varepsilon_x^b k_z^a\right)^2}\left(\chi_x^s - \frac{\varepsilon_x^a\varepsilon_x^b}{\epsilon_{ab}}\chi_z^s\right). \tag{A6}$$

[1] S. Yu, X. Wu, Y. Wang, X. Guo, and L. Tong, Adv. Mater. **29**, 1606128 (2017).

[2] F. Bonaccorso, Z. Sun, T. Hasan, and A. C. Ferrari, Nat. Photonics **4**, 611 (2010).

[3] A. C. Ferrari, F. Bonaccorso, V. Fal'ko, K. S. Novoselov, S. Roche, P. Boggild, S. Borini, F. H. L. Koppens, V. Palermo, N. Pugno *et al.*, Nanoscale **7**, 4598 (2015).

[4] K. F. Mak and J. Shan, Nat. Photonics **10**, 216 (2016).

[5] M. Bayle, N. Reckinger, A. Felten, P. Landois, O. Lancry, B. Dutertre, J.-F. Colomer, A.-A. Zahab, L. Henrard, J.-L. Sauvajol *et al.*, J. Raman Spectrosc. **49**, 36 (2017).

[6] D. S. L. Abergel, A. Russell, and V. I. Fal'ko, Appl. Phys. Lett. **91**, 063125 (2007).

[7] S. M. Eichfeld, C. M. Eichfeld, Y.-C. Lin, L. Hossain, and J. A. Robinson, APL Mater. **2**, 092508 (2014).

[8] H. Li, J. Wu, X. Huang, G. Lu, J. Yang, X. Lu, Q. Xiong, and H. Zhang, ACS Nano **7**, 10344 (2013).

[9] L. Ottaviano, S. Palleschi, F. Perrozzi, G. D'Olimpio, F. Priante, M. Donarelli, P. Benassi, M. Nardone, M Gonchigsuren, M. Gombosuren *et al.*, 2D Mater. **4**, 045013 (2017).

[10] T. Stauber, N. M. R. Peres, and A. K. Geim, Phys. Rev. B **78**, 085432 (2008).

[11] M. Lobet, B. Majerus, L. Henrard, and P. Lambin, Phys. Rev. B **93**, 235424 (2016).

[12] L. A. Falkovsky, J. Phys.: Conf. Ser. **129**, 012004 (2008).

[13] B. Majérus, M. Cormann, N. Reckinger, M. Paillet, L. Henrard, P. Lambin, and M. Lobet, 2D Mater. **5**, 025007 (2018).

[14] F. J. Nelson, V. K. Kamineni, T. Zhang, E. S. Comfort, J. U. Lee, and A. C. Diebold, Appl. Phys. Lett. **97**, 253110 (2010).

[15] S. Cheon, K. D. Kihm, H. G. Kim, G. Lim, J. S. Park, and J. S. Lee, Sci. Rep. **4**, 6364 (2014).

[16] J. P. Lu, Phys. Rev. Lett. **79**, 1297 (1997).

[17] P. Wagner, V. V. Ivanovskaya, M. J. Rayson, P. R. Briddon, and C. P. Ewels, J. Phys.: Condens. Matter **25**, 155302 (2013).

[18] M. Merano, Phys. Rev. A **93**, 013832 (2016).

[19] L. Matthes, O. Pulci, and F. Bechstedt, Phys. Rev. B **94**, 205408 (2016).

[20] G. Jayaswal, Z. Dai, X. Zhang, M. Bagnarol, A. Martucci, and M. Merano, Opt. Lett. **43**, 703 (2018).

[21] I. Valuev, S. Belousov, M. Bogdanova, O. Kotov, and Y. Lozovik, Appl. Phys. A **123**, 60 (2016).

[22] Y. Li and T. F. Heinz, 2D Mater. **5**, 025021 (2018).

[23] S. Funke, B. Miller, E. Parzinger, P. Thiesen, A. W. Holleitner, and U. Wurstbauer, J. Phys.: Condens. Matter **28**, 385301 (2016).

[24] V. G. Kravets, A. N. Grigorenko, R. R. Nair, P. Blake, S. Anissimova, K. S. Novoselov, and A. K. Geim, Phys. Rev. B **81**, 155413 (2010).

[25] A. G. Marinopoulos, L. Reining, A. Rubio, and V. Olevano, Phys. Rev. B **69**, 245419 (2004).

[26] E. Dremetsika and P. Kockaert, Phys. Rev. B **96**, 235422 (2017).

[27] K. S. Novoselov, A. Mishchenko, A. Carvalho, and A. H. Castro Neto, Science **353**, aac9439 (2016).

[28] F. A. Rasmussen and K. S. Thygesen, J. Phys. Chem. C **119**, 13169 (2015).

[29] R. M. A. Azzam, *Ellipsometry and Polarized Light* (North-Holland, Amsterdam, 1987), Sec. 4.6.

[30] J. E. Sipe, J. Opt. Soc. Am. B **4**, 481 (1987).

[31] B. U. Felderhof and G. Marowsky, Appl. Phys. B **44**, 11 (1987).

[32] See Supplemental Material at http://link.aps.org/supplemental/10.1103/PhysRevB.98.125419 for the calculation of the anisotropic transfer matrix of a single sheet.

[33] D. E. Aspnes, J. B. Theeten, and F. Hottier, Phys. Rev. B **20**, 3292 (1979).

[34] R. A. Depine, *Graphene Optics: Electromagnetic Solution of Canonical Problems* (Morgan and Claypool, San Rafael, California (USA), 2016), Chap. 2.

[35] M. N. Polyanskiy, Refractive index database, https://refractiveindex.info/?shelf=glass&book=BK7&page=SCHOTT.

[36] P. Blake, E. W. Hill, A. H. Castro Neto, K. S. Novoselov, D. Jiang, R. Yang, T. J. Booth, and A. K. Geim, Appl. Phys. Lett. **91**, 063124 (2007).